PB-227 109

GROWTH OF FINGERS AT AN UNSTABLE DIFFUSING INTERFACE IN A POROUS MEDIUM

Robin A. Wooding

California Institute of Technology

Prepared for:

Federal Water Pollution Control Administration

March 1969

DISTRIBUTED BY:

NTIS

National Technical Information Service
U. S. DEPARTMENT OF COMMERCE
5285 Port Royal Road, Springfield Va. 22151

PB 227 109

Tech. Memo 69-5

GROWTH OF FINGERS AT AN UNSTABLE DIFFUSING INTERFACE IN A POROUS MEDIUM

by

Robin A. Wooding

Supported by Research Grant No. 16000DGY
Federal Water Pollution Control Administration
U. S. Department of the Interior
and
Commonwealth Scientific and Industrial Research Organization
of Australia

W. M. Keck Laboratory of Hydraulics and Water Resources
Division of Engineering and Applied Science
California Institute of Technology
Pasadena, California

Technical Memorandum 69-5

March 1969

Reproduced by
NATIONAL TECHNICAL
INFORMATION SERVICE
U S Department of Commerce
Springfield VA 22151

Foreward

In the future, quality management of ground waters will depend on better knowledge of natural mixing phenomena in porous media. As in the atmosphere, lakes and oceans, it is possible to have convective instabilities in ground water masses when heavier water (colder or more saline) is introduced or recharged above a slightly lighter layer. In large open bodies of water the convection mixing proceeds fairly rapidly when fluids are hydrostatically unstable, because there is little internal resistance. On the other hand in ground water there is considerable resistance to convective overturning, and rates are much slower.

This paper is a contribution to the basic hydrodynamics of interfacial instability in stratified flow in porous media. The instability develops as a group of fingers, as demonstrated by both theory and experiment.

N. H. Brooks

Acknowledgments

The analytical work was supported primarily by Grant No. 16000DGY, Federal Water Pollution Control Administration (U.S.A.), during the author's temporary research appointment at the California Institute of Technology (W. M. Keck Laboratory of Hydraulics and Water Resources). Experimental work was performed at Commonwealth Scientific and Industrial Research Organization, Canberra, Australia. The numerical computations described in Section 5 were performed on the C.S.I.R.O. CDC 3600 Computer.

This paper has been submitted in somewhat abbreviated form to the Journal of Fluid Mechanics for possible publication.

R.A.W.

Table of Contents

	Page
Abstract	1
1. Introduction	2
2. Experimental Observations Using Hele-Shaw Cells	6
3. Approximate Equations of Finger Growth	12
4. Similarity Solutions	15
5. Numerical Solution of the Approximate Equations	19
6. Conclusions	24
References	25
Tables	26-34
Figures	35-45

ABSTRACT

Waves at an unstable horizontal interface between two fluids moving vertically through a saturated porous medium grow rapidly to become "fingers", when the amplitude greatly exceeds the wavelength. For a diffusing interface, it is observed experimentally that the mean amplitude taken over many fingers grows approximately as $(\text{time})^2$, followed by a transition to a growth proportional to time. Correspondingly, the mean wavenumber decreases approximately as $(\text{time})^{-\frac{1}{2}}$. The rapid increase of amplitude implies that longitudinal dispersion becomes negligible relative to wave growth. To represent the observed average quantities, the transport equation is weighted and averaged over the horizontal plane. Hyperbolic equations result, and the ascending and descending zones containing the fronts of the fingers are replaced by discontinuities. Relations between wavenumber and amplitude are derived from similarity assumptions. The amplitude is fairly insensitive to wavenumber changes. Numerical solutions of the averaged equations give fairly detailed information on the growth behaviour, in excellent agreement with the similarity results and with experiment.

1. INTRODUCTION

Although flows in porous media generally involve extremely low Reynolds numbers (the so-called Darcy flows), the existence of several mechanisms which could induce instability has been recognized for many years (Horton and Rogers 1945, Lapwood 1948, Saffman and Taylor 1958). In particular, most of these effects can appear in the instabilities associated with an interface between two fluids in a porous medium.

Immiscible fluids

Saffman and Taylor (1958) pointed out that the instability which may arise at a moving interface between two immiscible fluids in a porous medium possesses analogies to Taylor instability (Taylor 1950). They considered a small perturbation (of wave number α) to a horizontal interface, when the steady state was one of uniform fluid velocity W upwards, and showed that the initial growth law was proportional to $\exp(2\Lambda^* \alpha T)$. Here T is time and

$$2\Lambda^* \left[\frac{\mu_1}{k_1} + \frac{\mu_2}{k_2} \right] = g(\rho_1 - \rho_2) + \left[\frac{\mu_1}{k_1} - \frac{\mu_2}{k_2} \right] W \qquad (1)$$

in which ρ and μ refer to the fluid density and viscosity, while k denotes permeability of the medium and g denotes gravity. The suffixes 1 and 2 refer to the upper and lower fluids respectively. Saffman and Taylor noticed that a thin film of the displaced fluid 1 tends to adhere to the surfaces of the porous medium thus reducing the effective permeability to fluid 2, i.e. $k_2 < k_1$. Also, expression (1) requires modification when interfacial tension effects are present (Chuoke, van Meurs and van der Poel 1958).

In an extension of their work, Saffman and Taylor treated the growth of large-amplitude waves, or "fingers", at the interface between immiscible fluids in a Hele-Shaw cell. For this limiting case the amplitude, measured from the centre of a finger, is $\Lambda^* T$, and the flow within the finger is uniform.

Miscible fluids

When the interface is formed between two fluids which can interdiffuse, the problem acquires two length scales - the growing

thickness $(\kappa T)^{\frac{1}{2}}$ of the interface, where κ is an appropriate diffusivity, and the "natural" length scale κ/Λ, where Λ is a velocity analogous to Λ^*.

For the instability problem, Elder (1968) observed that there were analogies with both Taylor and Rayleigh instability mechanisms, and suggested that the most rapidly amplified waves involved wavelengths comparable with the thickness of the diffusion layer. (See also Heller 1966)

Elder carried out numerical experiments on the early growth of instabilities at various types of thermal interface, including the sublayer at a heated horizontal boundary within a porous medium. The latter case is of particular interest here, and may be summarized briefly as follows.

1. After a rapid initial development, a small almost-steady induced flow exists due to thermal "noise" already present in the system.

2. In the next stage the growth of the disturbance is closely exponential, with exponent proportional to the square of the Rayleigh number. (It can be shown from this growth law that the disturbance wavenumber is scaled as Λ/κ.) In this régime the amplitude increases by at least one order of magnitude.

3. The system changes to one of approximately constant acceleration, with velocities increasing linearly with time and displacements, presumably, increasing as the square of the time. A further order-of magnitude increase in amplitude occurs, the disturbance attaining a magnitude of at least O(1); thus this régime is distinctly non-linear and the form of the sublayer is modified considerably.

In Elder's view, the acceleration arises because progressively more buoyant fluid from deeper inside the sublayer is drawn into the disturbance (which now resembles a series of "blobs"), thus increasing the effective density difference. This process continues until the sublayer is largely removed.

Elder's numerical results are particularly valuable because they cover a range which is extremely difficult to observe experimentally. Although the case of a free interface in a porous medium is not treated, much of the above qualitative discussion should be applicable without major modification.

By comparison, the behaviour of large-amplitude waves, or fingers, is simple to observe experimentally, but may be difficult to treat numerically. Thus a series of experimental observations can cover the important range of disturbance growth at large times, which is the topic of this paper. Such a study does not lead to a fully determinate model since the initial perturbation solution is unknown. However, a good deal may be learned about the properties of the system without specifying the full initial-value problem.

The equations of the flow

For flows of inhomogeneous fluids at very low Reynolds number (defined relative to pore dimension) in a porous medium, the appropriate general equations are given below:

Continuity: $$\nabla \cdot \underset{\sim}{q} = 0 \qquad (2)$$

where $\underset{\sim}{q}$ is the volume flow vector

Darcy's equation: $$\nabla P - \rho \underset{\sim}{g} + \frac{\mu}{k} \underset{\sim}{q} = 0 \qquad (3)$$

where P is pressure, $\underset{\sim}{g}$ is the gravity vector, k is the permeability of the medium, and ρ and μ are the density and viscosity of the fluid.

Mass transport: $$\epsilon \rho_T + \underset{\sim}{q} \cdot \nabla \rho = \nabla \cdot (\underset{\sim}{\kappa} \nabla \rho) \qquad (4)$$

Here ϵ is the porosity and $\underset{\sim}{\kappa}$ is the difusivity tensor, and T is time.

It is convenient to take X and Y axes in the plane of an assumed initially-horizontal interface, having the origin moving with the interface, and the Z axis directed vertically upwards. Now, if there is a uniform constant superposed flow W_o upwards, the velocity of the interface will be W_o/ϵ. If $\underset{\sim}{q} = (U, V, W)$ relative to the above axes, it is found that the equations (2) to (4) are unchanged in form except that the left-hand side of (3) contains a resistance term $\mu W_o/k$ acting in the Z-direction.

For the non-linear problem posed by the system when the wave amplitude is large, it will be assumed that the following decomposition of the density profile can be made. Let the density of the upper fluid be $\rho_o + \Delta$, of the lower fluid $\rho_o - \Delta$. Further, let $\overline{\rho}(Z, T)$ be the mean density on the X, Y plane at height Z, so that

$$\rho = \left\{ \rho(X, Y, Z, T) - \overline{\rho}(Z, T) \right\} + \left\{ \overline{\rho}(Z, T) - \rho_o \right\} + \rho_o$$

$$= \rho_o + (\varphi + \theta)\,\Delta \qquad (5)$$

where $\varphi(Z, T) = \dfrac{\overline{\rho} - \rho_o}{\Delta}$ and $\theta(X, Y, Z, T) = \dfrac{\rho - \overline{\rho}}{\Delta}$

are dimensionless variables. Note that φ represents the variation of the mean density at height Z from the central value ρ_o, while θ represents point fluctuations of density relative to the mean value over the plane at the given value of Z.

Variation of visoosity μ with density will be represented approximately by the first two terms of a Taylor expansion

$$\mu \approx \mu_o \left\{ 1 + \frac{\Delta}{\mu_o} \left[\frac{d\mu}{d\rho}\right]_o (\varphi + \theta) \right\} \qquad (6)$$

where the factor $(\Delta/\mu_o)\ (d\mu/d\rho)_o$ will be assumed small relative to unity. It is thus appropriate to apply the Boussinesq approximation with regard to μ.

Finally, for the pressure, let

$$P = \overline{P}(Z, T) + p(X, Y, Z, T) \qquad (7)$$

where $\overline{P}$ is the mean pressure over a plane at distance Z from the interface and p represents point fluctuations of pressure over the plane.

If the variables defined in (5) to (7) are substituted into Darcy's equation (3) and $\overline{P}$ is eliminated, the result is

$$\frac{k}{\mu_o} \nabla p + (0, 0, \Lambda\,\theta) + \underset{\sim}{q} = 0 \qquad (8)$$

where

$$\Lambda = \frac{k\,g\,\Delta}{\mu_o} + \frac{\Delta}{\mu_o} \left[\frac{d\mu}{d\rho}\right]_o W_o \qquad (9)$$

is defined to be the characteristic velocity for miscible fluids, analogous to the parameter Λ^* given in (1) for the immiscible case. Now, let $(u, v, w) = \underset{\sim}{q}/\mathbf{A}$ be a dimensionless flow vector. Elimination of p from (8) gives

$$\nabla_1^2 \theta + \nabla^2 w = 0 \tag{10}$$

in which ∇_1^2 signifies $\partial^2/\partial X^2 + \partial^2/\partial Y^2$.

In the equation of mass transport, it is necessary to make some assumption about the nature of the diffusivity tensor. Since the applied flow rate W_o is directed normal to the interface, it will be assumed that there is a coefficient of longitudinal diffusion and dispersion κ_ℓ in the direction of W_o, and a coefficient of transverse diffusion and dispersion $\kappa_t (\leq \kappa_\ell)$ in any direction normal to W_o. Both of these will be taken to be at least approximately constant. Then the diffusion term can be simplified. If all the dependent variables are now represented by dimensionless quantities, (4) can be written

$$\varphi_S + u\,\theta_X + v\,\theta_Y + w\,\theta_Z - \frac{\kappa_\ell}{\Lambda}\,\varphi_{ZZ}$$

$$+\ \theta_S + w\,\varphi_Z - \frac{\kappa_t}{\Lambda}\,\nabla_1^2\,\theta - \frac{\kappa_\ell}{\Lambda}\,\theta_{ZZ} = 0 \tag{11}$$

where $S = \Lambda T/\epsilon$ is a stretching length scale analogous to the amplitude of fingers growing between two immiscible fluids (cf. section 1).

The equations (10) and (11), with the equation of continuity, could be replaced by difference equations for numerical solution, as was done by Elder (1968) for two-dimensional flow. Here, however, a form of spatial averaging will be introduced (section 3) in order to simplify the system. The experimental observations which assist in formulating this approach are described in section 2.

2. EXPERIMENTAL OBSERVATIONS USING HELE-SHAW CELLS

For visual studies on flow through porous media, the Hele-Shaw cell has been used by several workers, e.g. Saffman and Taylor (1958), Elder (1967), Wooding (1963). Some non-typical flows may be

encountered which interfere with simulation, notably the effects of interfacial tension between immiscible fluids mentioned in section 1. These difficulties are not likely to arise when the fluids are miscible solutions which differ only slightly in their physical properties.

Lamb (1932) has summarized the theory of Hele-Shaw flow for a homogeneous fluid. Let rectangular co-ordinates be taken in the plane of a cell sloping at an angle β to the horizontal, with the Z-axis directed up the line of greatest slope and the X-axis horizontal; the fluid velocity averaged across the space between the plates at a given point (X, Z) is

$$(U, W) = - (h^2/12\mu) (\partial/\partial X, \partial/\partial Z) (P + g \rho Z \sin \beta) \qquad (12)$$

where h is the spacing between the plates, P is the pressure, ρ and μ are the density and viscosity of the fluid and g sin β is the gravity component in the plane of the cell. If $k = h^2/12$ is the equivalent permeability, (12) is equivalent to the equation of motion for a two-dimensional flow of incompressible fluid in a porous medium.

When a Hele-Shaw cell is used to simulate the flow of non-homogeneous fluid in a porous medium, it is generally assumed that the fluid properties are slowly-varying functions of the space co-ordinates; that is, the variation in fluid properties should be negligible over a distance in the (X, Z)-plane comparable with the plate spacing h. It has been noted (Wooding 1960) that the longitudinal dispersion observed in a Hele-Shaw cell should be represented approximately by the calculated Taylor dispersion (Taylor 1953). The formula for flow between parallel planes is

$$\kappa_\ell = \kappa + \frac{1}{210} \frac{W^2 h^2}{\kappa} \qquad (13)$$

where κ is the molecular diffusivity. In the present problem, most dispersion is likely to occur in the Z-direction when there is a superimposed velocity W_o.

At the present time, a precise analysis is lacking for flow of non-homogeneous fluids in a Hele-Shaw cell. However, experimental work with an analogue of the two-dimensional laminar Schlichting jet

(Wooding 1963) appears to show that the analogy is extremely close. In these experiments, measurements were made of the distance of advance (Z_m say) of the leading edge of a dense laminar "starting plume" in a Hele-Shaw cell. In the established part of the plume the velocities and density can be calculated by Schlichting's (1933) theory; in particular, the fluid velocity, W_m say, on the axis of the plume is known. In this way it was found that

$$\frac{dZ_m}{dT} = 0.33\, W_m \qquad (14)$$

A relation of this form would be expected from similarity provided that Schlichting's theory is obeyed.

Experimental Method

Two Hele-Shaw cells were constructed from sheets of 1/4" thick polished plate glass, having internal boundaries (impermeable to water flow) made from thicknesses of rubber insulating tape. Figure 1(a) shows the arrangement. Two impermeable tape boundaries parallel to the Z-direction and separated by a known distance were stuck permanently to one sheet of glass, and served also to control the spacing of the glass. A horizontal removable strip, passed through a slot cut in one permanent boundary, was used to divide the cell into equal upper and lower portions. The first (smaller) cell was not closed at the bottom, mainly in order to achieve satisfactory pressure equalization on the two sides of the removable strip, but the second cell was closed as shown in the figure.

Initial filling of the cell was carried out by immersing both plates in distilled water in a transparent tiltable tank (figure 1b,c) and then clamping the plates together with the removable strip in place. The upper half of the cell, above the removable strip, was filled with dilute potassium permanganate solution, using a fine glass capillary tube thin enough to pass between the plates. This provided a source of fluid about 5 cm. from the top of the cell. The strength of the source was adjusted to provide a broad two-dimensional plume (Wooding 1963) which consists of a core of uniform undiluted solution bounded by a mixing layer of either side. As would be expected, the upper edge of the solution

consisted of dispersed fluid exhibiting a gradual change of density with height. However, this mixed zone was forced to the top of the cell during the filling process, away from the neighbourhood of the region of interest. The filling process was usually carried out with $\beta \approx 10^{\circ}$. After filling had been completed, the cell would be left to stand for about 12 hours (at $\beta \approx 5^{\circ}$) to permit any density irregularities near the top of the cell to become smoothed out by convection and diffusion.

To initiate an experiment, the removable strip was withdrawn steadily to one side of the cell when the latter was in a nearly horizontal position. Then the cell was tilted quickly to a pre/selected value of β, and the time measured from that point. Photographs were taken at suitable intervals to record the growth of waves on the unstable interface. Inevitably, removal of the central strip left some space which had to be filled by movement of fluid into the cell. However, since the motion was necessarily a non-inertial (Stokes) flow because of the small spacing of the plates, little mixing appeared to be induced at this stage.

The photographic sequence of figure 2(a) shows the features generally recorded with the growth of waves at the unstable interface. After formation of the interface, some little time elapses before a large number of small waves appear. These grow rapidly, and the amplitude presently becomes greater than the wavelength. The waves have developed the character of "fingers", resembling those observed by Saffman and Taylor (1958) and Chuoke, van Meurs and van der Poel (1958).

As the sequence of photographs also shows, the number of fingers appears to diminish with time. In fact, inspection of the later frames in figure 2(a) leads to the suggestion that the fingers spread laterally with time. There is a tendency for adjacent waves to coalesce by mutual entrainment - a process controlled by diffusion - thus decreasing the apparent wavenumber. Elder (1968) notes a similar effect which he calls "the amalgamation of eddies". The process of waves, or fingers, growing and slowly spreading must result in considerable mutual interference; hence the irregularity of the pattern seen in figure 2 is not surprising.

An additional complicating feature is important and deserves mention. At an advanced stage of development of the fingers, the fronts

tend to become unstable and break into two separate fingers (figure 2(b)). Thus the process of wavenumber decrease is arrested. A similar instability has been noted in connection with the dense starting plume described earlier in this section.

Because of the irregularities in the pattern of growing fingers, only statistical averages were extracted from the photographs. The mean wavelength was obtained by counting the total number of growing wave crests and troughs visible on each photograph, and dividing this number into twice the width of the cell. Elder (1968) used a similar method. Naturally, the estimate of the mean improves as the number of fingers increases, and the measurements using the larger cell (II) show appreciably less scatter than those with cell I. To measure the mean amplitude, or half-length of finger, an envelope was sketched around the pattern, touching the crests on one side and the troughs on the other, and the area of the envelope measured with a planimeter.

Experimental Parameters and results.

Table I gives the dimensions of the two Hele-Shaw cells used. The table also shows that fairly dilute solutions of potassium permanganate were used; at the relatively high permeabilities of the two Hele-Shaw cells, it was necessary to use a low density contrast so that the disturbance growth was slow enough to be recorded conveniently.

Quite different values of equivalent permeability and solution density applied in the two cells, in addition to the differences in size. For this reason, the two experiments recorded using cell I are included in the data as useful comparisons, although the experiments with this cell were fairly rough.

The value of Λ for each experiment was calculated from the formula

$$\Lambda = \frac{\rho_s - \rho_w}{2} \cdot \frac{kg \sin \beta}{\mu} \qquad (15)$$

based on (9), where ρ_s and ρ_w are densities of solution and water respectively, and k is the equivalent permeability obtained from table 1. The values of the dynamic viscosity μ and density ρ_w were obtained from tables for water (Dorsey 1940) appropriate to the measured mean temperature in each experiment.

Summaries of the data measured in photographic sequences from seven experiments - two of these in cell I and five in cell II - are plotted in figures 3 and 4 as mean wave-length versus time and as mean amplitude versus the quantity ΔT respectively. A key to the plotting symbols used is given in table 2. This table also shows that the experimental Λ-values covered a range of about 16 to 1.

From figure 3, the mean-wavelength measurements tend towards a line defined by

$$0.0190 T^{\frac{1}{2}} \approx 2\pi(\kappa T)^{\frac{1}{2}} / 0.827 \qquad (16)$$

in C.G.S. units, where the diffusivity value κ has been taken from table 1. It is worth noting that the mean wavenumber is close to $(\kappa T)^{-\frac{1}{2}}$. Since, as will be shown later, longitudinal diffusion is not significant at large time, a tentative conclusion is that transverse diffusion is a controlling factor, giving an apparent wavenumber which decreases with time due to the decay of fingers with high wavenumbers.

Many of the points measured early in an experiment lie above the full line in figure 3, and these indicate that the mean wavenumber is relatively lower at that stage.

A different situation may apply for one set of experimental data (that indicated by the broken line in figure 3) which lies entirely above the main line. In fact, this experiment was carried out in Hele-Shaw cell I which was open at both ends, so that an appreciable convective flow was taking place through the cell due to the excess density of the solution. The calculated mechanical dispersion was found to be roughly 3 times the molecular diffusivity, so that the initial wavenumber could be significantly lower.

Figure 4 illustrates clearly the remarkably close scaling of amplitude with the time-like length variable $S = \Delta T/\epsilon$. Although the previous figure has shown that the observed wavelength is very sensitive to

changes in diffusivity, it is apparent that the effect upon amplitude is at most slight. A similar conclusion was reached by Slobod and Thomas (1963) who examined unstable miscible-phase displacement in a porous plate at two different flow rates.

In spite of experimental scatter, the present observations of amplitude define fairly well a pair of lines obeying the relations

$$Z_m = 0.0732\ S^2 \quad (S < 6.1 \text{ cm}) \qquad (17)$$

and

$$Z_m = 0.446\ S \quad (S > 6.1 \text{ cm}) \qquad (18)$$

respectively, where Z_m is the mean amplitude in cm. measured relative to the origin of co-ordinates. From the first relation, it appears that these experimental results overlap the final phase (3 in section 1) of Elder's (1968) numerical experiments. The second relation (18) is particularly interesting since the limiting growth rate for an immiscible finger is $Z_m = S = \Delta T$. Thus the miscible-fluid fingers are growing at less than one-half of that rate, suggesting that the density distribution across a finger resembles a diffusion profile, as would be expected if transverse diffusion and associated fluid entrainment were taking place.

A further consideration is the observed instability of the fronts of well-developed fingers. Since this phenomenon is also observed with the dense starting plume, it appears to be associated with an increase in transverse length scale. A qualitative resemblance to the starting plume is therefore apparent.

3. APPROXIMATE EQUATIONS OF FINGER GROWTH

A detailed analysis of the growth problem is not attempted in this paper, but some of the observed average properties of large-amplitude fingers may be derived from the equations (2), (10) and (11) of section 1. Of these equations, it will be noted that only (11) is non-linear, and that the equation naturally falls into two parts, the first five terms being either independent of X and Y, or nearly so, while the remaining four terms are quasi-periodic in these variables.

For large S, the ratio of terms involving Φ_{ZZ} and Φ_S

respectively in equation (11) is $O(\kappa_t S/\Delta Z^2)$. Hence, if a typical Z-scale increases more rapidly than $S^{\frac{1}{2}}$, as the experimental results show, then the term in φ_{ZZ} may be neglected for large S. A consideration of numerical values appropriate to the experimental work indicates, for each case, that this approximation may be assumed valid for all of the recorded measurements. A similar argument to the above applies to the term involving θ_{ZZ}. In equation (10) the situation is a little different; if it is assumed that a typical scale in the X, Y-plane does <u>not</u> increase more rapidly than $S^{\frac{1}{2}}$, again in agreement with experiment, then ultimately w_{ZZ} becomes negligible relative to $\nabla_1^2 w$ and (10) may be integrated to give

$$\theta + w = 0 \qquad (19)$$

<u>Equations governing averaged quantities</u>

Now suppose that the saturated porous medium is bounded by a cylindrical container of arbitrary cross-section and with vertical impermeable sides. Upon these sidewalls the boundary conditions are $u = w_n = 0$, where the suffix n signifies the normal derivative. However, if it is also assumed that the cross-section is large enough to contain many fingers, the influence of sidewalls upon quantities such as hroizontal wavenumber will be small. When (19) is used to eliminate θ from (11) and the latter equation is averaged over the entire cross-section at a given value of Z, the result is

$$\varphi_S = \overline{w^2}_Z \qquad (20)$$

assuming that quasi-periodic terms disappear when averaged over a large number of waves. Again, let (11) be multiplied by $w / (\overline{w^2})^{\frac{1}{2}}$ and the average taken over the same cross-section, to give

$$(\overline{w^2})^{\frac{1}{2}}{}_S = (\overline{w^2})^{\frac{1}{2}} \left\{ \varphi_Z - \frac{\kappa_t}{\Lambda} \alpha^2 (Z, S) \right\} \qquad (21)$$

where α is an "equivalent mean wavenumber" - a slowly-varying function of Z and S - defined by

$$\alpha^2 \overline{w^2} = \overline{w_X^2} + \overline{w_Y^2} \qquad (22)$$

It must be assumed that the observed mean wavenumber does not differ greatly from this quantity. Subsequent results based upon these equations appear to show that (21) has been expressed in the correct "conservative form". The possibility of non-uniqueness has been discussed by Lax (1954).

Equations corresponding to (20), and (21) have been derived for the problem of flow in a vertical tube filled with porous material (Wooding 1962). In that case, a reasonable approximation could be made for the shape of the transverse density profile governed by the tube geometry, leading to an estimate for the dominant wavenumber α. No such criterion exists in the present case since $\overline{w_X^2}$ and $\overline{w_Y^2}$ are not known. Information on α might be sought from additional equations, obtained by suitable weighting of (11) with derivatives of w and averaging over X, Y. However, this introduces unknown terms of higher orders and increases the complexity of the system. In this paper the behaviour of α will be inferred from considerations of similarity.

Characteristic form of the equations

As already observed (Wooding 1962), the differential equations (20) and (21) form a hyperbolic system, and can be written in the characteristic form

$$\frac{dZ}{dS} = \pm (2\,\overline{w^2})^{\frac{1}{2}} \qquad (23)$$

$$\frac{d}{dZ}\left\{\varphi \mp (2\,\overline{w^2})^{\frac{1}{2}}\right\} = \frac{\kappa_t}{\Lambda}\alpha^2(Z, S) \qquad (24)$$

the upper signs referring to ascending characteristics and the lower signs to descending characteristics. Equations (23) and (24) show that the system possesses a high degree of symmetry.

Jump conditions

The possibility of discontinuities arising in φ and $\overline{w^2}$, corresponding to the fronts of fingers, has been considered previously (Wooding 1962).

In the present problem it is necessary to suppose that all fingers extend approximately to the average height $Z_m(S)$ (above the plane Z = 0), and this will be taken to be the location of the discontinuity. Let φ_o denote the dimensionless density just ahead of the advancing fingers and assume that $\overline{w_o^2} = 0$ there, i.e. that the fluid is not in motion. Let the

suffix m denote any quantity measured just behind the jump.

If (20) is integrated over a short interval in Z which contains Z_m, the limit result is

$$U(S) \left\{ \varphi_o(S) - \varphi_m \right\} = \overline{w_m^2} \qquad (25)$$

where $U = dZ_m/dS$ is the jump "velocity" referred to S and the S-variation of φ_o is actually induced by the motion of the fingers advancing into the still fluid. From (21), similarly, using (20),

$$U^2(S) = \frac{2}{3} \overline{w_m^2} \qquad (26)$$

In summary, (25) and (26) give

$$\frac{3}{2} \frac{dZ_m}{dS} = \frac{3}{2} U(S) = \varphi_o(S) - \varphi_m = \pm \left[\frac{3}{2} \overline{w_m^2} \right]^{\frac{1}{2}} \qquad (27)$$

the positive and negative signs on the right applying for ascending and descending jumps respectively.

The characteristic equations (23) and (24) with jump conditions (27) illustrate the symmetry of the system. If the initial distribution of density (φ_o) is antisymmetric about the plane Z = 0, the two sets of characteristics are mirror images in the axis Z = 0 of the (Z, S)- plane.

4. SIMILARITY SOLUTIONS

The power-law growth of finger amplitude observed in experiments suggests that the more obvious features of the system behaviour might be modelled by assuming similarity solutions of relatively simple type. Let

$$\left.\begin{aligned} \zeta &= \frac{L^{q-1} Z}{S^q} , \\ \varphi &= (S/L)^{q-1} F(\zeta) , \\ 2\overline{w^2} &= (S/L)^{2q-2} G^2(\zeta) \end{aligned}\right\} \qquad (28)$$

where L is an arbitrary length scale and q is an unspecified exponent.

Then (20) and (21) become a pair of simultaneous non-linear ordinary differential equations.

$$q \zeta F' + G G' = (q-1) F \qquad (29)$$

$$G F' + q \zeta G' = (q - 1 + \gamma) G \qquad (30)$$

in which $$\gamma (Z, S) = \frac{\kappa_t}{\Lambda} S \alpha^2 (Z, S) \qquad (31)$$

The S-dependence of α^2 is not known a priori; however, for (29) and (30) to be independent of S it is necessary either (I) that the right hand side of (31) should be negligible, or (II) that $S \alpha^2$ should be independent of S. Case I is probably not of direct interest here because it can only result from waves which, by equation (1), would have very slow rates of initial growth. In any event the α^2 term in (31) will ultimately become significant for large enough S. If a disturbance growth based upon a power law developes, then II must apply and $\alpha \sim S^{-\frac{1}{2}}$, in accordance with the experimental observations.

An additional complication arises from the unknown ζ-dependence of α^2, and hence of γ. However, the main solution properties are unlikely to be greatly affected by slow variations of this factor and, for convenience, γ will be assumed constant.

In terms of the new variables defined in (28), the jump conditions (27) become

$$\tfrac{3}{2} q \zeta_m = F_o - F_m = \pm \tfrac{1}{2} 3^{\frac{1}{2}} G_m \qquad (32)$$

where $$F_o = \left(\frac{L}{S}\right)^{q-1} \varphi_o(S) \qquad (33)$$

Since F_o must be independent of S, it is evident that $\varphi_o \propto S^{q-1}$; if the power-law dependence of φ_o upon S is known, q may be determined, or vice versa. Also, as $\zeta = \zeta_m$ = constant at the jump, (28) gives $Z_m \propto S^q$ for the growth rate. The experimental results of figure 4 indicate the existence of a flow régime with $q \approx 2$ and a later régime with $q \approx 1$. A finite transition zone probably separates these two power-law régimes.

Similarity properties when q = 1

For the case of fingers advancing into homogeneous still fluid,

$\varphi_o(S) = 1$ in (33) so that $q = 1$, $F_o = 1$ and the unknown length L disappears. Then F can be eliminated from (24) and (25) to give

$$G' = -\gamma \Big/ \left[\frac{G}{\zeta} - \frac{\zeta}{G} \right] \tag{34}$$

The appropriate solution of (34) is

$$\begin{aligned} F/C_1 &= \tfrac{1}{2}\gamma \int_o^t t^{-\frac{1}{2}} \{1 + (\gamma-1)t\}^{-\frac{3\gamma-2}{2\gamma-2}} dt \\ G/C_1 &= \{1 + (\gamma-1)t\}^{-\frac{\gamma}{2\gamma-2}} \end{aligned} \tag{35}$$

where the parameter $t = \zeta^2/G^2$ (36)

Here F and G are odd and even functions of ζ respectively, as required by the symmetric nature of the problem. The constant C_1 of integration appears as a scale factor because of homogeneity in the ratios $F : G : \zeta$. Solution curves of F/C_1 and G/C_1, taking positive ζ/C_1 as abscissa, are given in figure 5(a) for selected values of the parameter γ.

Figure 5(a) may be used to obtain a graphical solution of the system of equations (35) and (36) subject to the discontinuity conditions (32). There are four relations available for the five quantities γ, C_1, F_m, G_m and ζ_m; the problem could be rendered unique if either γ or ζ_m, for example, were known from appropriate initial conditions. In figure 6 the dependence of F_m, G_m and $\gamma = \gamma_1$ upon ζ_m is shown.

A single point - a mean result from the experiments described in section 2 representing the observed values of γ_1 and ζ_m - falls on the appropriate curve in the figure.

Figure 6 shows that, in general, ζ_m decreases as the mean wavenumber is increased - a result to be expected since a greater mean density gradient is required to maintain steady flow at higher wavenumbers. From equation (21), the condition for $(\overline{w^2})^{\frac{1}{2}}_S \Big/ (\overline{w^2})^{\frac{1}{2}}$ to be zero is given by

$$\varphi_Z = \frac{\kappa_t}{\Lambda} \alpha^2 (Z, S)$$

and this is formally identical to the linearized condition for neutral stability of a disturbance Fourier component with horizontal wavenumber α and zero vertical wavenumber. In terms of the similarity variables, the

criterion is equivalent to

$$F' = \gamma$$

Now, close to the centre of the finger system ($\zeta = 0$) the equations (29) and (30) give

$$F' = \gamma + O(\zeta^2)$$

for the dimensionless density gradient. That is, when $q = 1$ the mean density gradient at the centre of the fingers corresponds to the neutral value. It is also the point at which the gradient is a minimum.

It may be noted that, if $\gamma = \frac{2}{3}$, the value of $(\kappa T)^{\frac{1}{2}}$ times the wavenumber is $(2/3)^{\frac{1}{2}} \approx 0.816$, which differs from the experimental mean value of 0.827 by little over 1%, and (35) and (36) reduce to

$$F = 2\zeta/3G , \quad G = 1 - \zeta^2/3G^2 \qquad (37)$$

The solution is indicated by broken curves in figure 5(a). The corresponding value of ζ_m is 4/9 while $F_m = 1/3$, $G_m = (4/9)3^{\frac{1}{2}}$ and $C_1 = 3^{\frac{1}{2}}/2$.

The case $q = 2$

For this flow regime, Elder (1968) has suggested a physical model (3 in section 1) in which acceleration continues while fluid from the diffusion layer is being drawn into the fingers, thus progressively increasing the effective density difference. This implies that the dimensionless density function $\varphi_o(S)$ increases with S, but does not further specify its form. Since $q \approx 2$ from experiment, the inference from (33) is that $\varphi_o \propto S$, at least over a finite range of S. Therefore, put

$$\begin{aligned} \varphi_o(S) &= \pm S/L' && (S \leqslant L') \\ &= \pm 1 && (S > L') \end{aligned} \qquad (38)$$

the sign depending upon the direction of motion of the discontinuity. Here L' is a further length parameter.

The quantity ζ_m corresponds to the location of the discontinuity, and it is appropriate that its value should remain constant through both the q = 2 and q = 1 regimes of flow. Then, in (28), let L be taken equal to the value of S (= 6.1 cm.) at which the two experimental curves (17) and (18) intersect. It follows at once from the discontinuity conditions (32) that $(F_o - F_m) / q$ and G_m/q do not change when q changes, so that the quantities $F_o - F_m$ and G_m decrease by a factor of 2 at S = L. This corresponds to the difference in slope of the lines (17) and (18) at the point of intersection in figure 4.

For q = 2, the quantities F/C_2 and G/C_2 have been obtained as functions of ζ/C_2 by numerical integration of equations (29) and (30) (figure 5b) where C_2 is a new scaling constant. An attempt to fit graphically the jump conditions (32) to this solution gives $F_o = 2$ when q = 2, and (33) and (38) give $L' = \frac{1}{2}L$. Thus C_2 and γ can be determined as functions of ζ_m.

The dependence of $\gamma = \gamma_2$ as well as F_m/q and G_m/q upon ζ_m for q = 2 is shown in figure 6. This indicates that γ is smaller when q = 2 than when q = 1 in the relevant range of ζ_m. In fact, if $\zeta_m \approx 4/9$, $\gamma_2 \approx 4/9$, corresponding to a mean wavenumber about $(2/3)^{\frac{1}{2}}$ times that observed for the case q = 1. This result is in rough agreement with measurements made at early stages in most experiments (figure 3).

Transition regime

The observed increase in γ, between the regimes of q = 1 and 2, appears reasonable provided that the transition between them is characterized by a reduced rate of decrease of the wavenumber in the physical (X, Y) - plane, and if S at least doubles during the transition. Little can be deduced about the transition from similarity considerations, and it is examined in more detail in the context of a numerical solution (section 5).

5. NUMERICAL SOLUTION OF THE APPROXIMATE EQUATIONS

For a numerical solution using a high-speed digital computer, the system of hyperbolic equations (20) and (21), subject to jump conditions (27), is generally preferable to the characteristic form (23) and (24).

Let the equations be rendered fully non-dimensional by putting

$$s = S/L' \ , \quad z = Z/L' \ , \quad A^2(s) = \frac{\kappa_t \alpha^2 L'}{\Lambda} \tag{39}$$

and, for convenience, let $w' = (\overline{2w^2})^{\frac{1}{2}}$ (40)

Equations (20) and (21) become

$$\varphi_s = \tfrac{1}{2}(w'^2)_z \tag{41}$$

$$(\log w')_s = \varphi_z - A^2(s) \tag{42}$$

the form of (42) being the most suitable one for a finite-difference scheme (Fox 1962).

Instead of applying two sets of jump conditions located symmetrically with respect to z = 0, it is simpler to consider one-half of the flow field, say for $z \geq 0$, and to apply a symmetry condition on the axis. Then, from (27) and (38),

$$\frac{dz_m}{ds} = U = \frac{2}{3}\{\varphi_o(s) - \varphi_m\} = 3^{-\frac{1}{2}} w'_m \tag{43}$$

at $z = z_m$, where

$$\begin{aligned} \varphi_o(s) &= s \quad (0 < s \leq 1) \\ &= 1 \quad (s > 1) \end{aligned} \tag{44}$$

On z = 0, $\varphi = w'_z = 0$ (45)

Finite-difference method

An appropriate differencing scheme is due to Lax (1954). With reference to the rectangular mesh shown in figure 7(a), (41) and (42) are replaced by the forward-difference equations

$$\varphi_{i,2} = \tfrac{1}{2}(\varphi_{i-1,1} + \varphi_{i+1,1}) + \tfrac{1}{2}\frac{\Delta s}{2\Delta z}(w'^2_{i+1,1} - w'^2_{i-1,1}) \tag{46}$$

$$(\log w')_{i,2} = \tfrac{1}{2}\{(\log w')_{i-1,1} + (\log w')_{i+1,1}\} + \Delta s\{(\varphi_{i+1,1} - \varphi_{i-1,1})/(2\Delta z) - A^2(s)\} \tag{47}$$

The particular form of time difference chosen by Lax introduces a small artificial diffusion term with coefficient $(\Delta z)^2/2\Delta s$; it has the merit of stabilizing the equations and leading to physically meaningful solutions. (See also Fox 1962.) The mesh ratio $\Delta s/\Delta z$ must be chosen such that the diffusion coefficient is small; otherwise the solution drifts into error although there is adequate stability. A linearized analysis of the non-linear equations (46) and (47) gives the stability criterion

$$\Delta s/\Delta z \leq 1/w' \tag{48}$$

which, from (23), corresponds also to the Courant condition. It has been found by trial that a "square" mesh $\Delta s = \Delta z$ is appropriate in the present problem since $w' < 1$, and introduces little error from diffusion if the step length is suitably chosen.

To solve the problem of the advancing jump, an additional relation is needed between the quantities at the jump (Fox 1962). Keller, Levine and Whitham (1960) differentiate the jump velocity with respect to time. With this method (43) gives two alternative formulae. The one adopted here is

$$3^{\frac{1}{2}} \frac{dU}{ds} = \frac{dw'_m}{ds} = w'_m \{(\varphi_z)_m - A^2(s)\} + U(w'_z)_m \tag{49}$$

using (42).

Again, following Keller, Levine and Whitham, the equations at the jump are replaced by an implicit difference scheme using backward s-differences which is unconditionally stable. From (43), referring to figure 7(b),

$$z_{m,2} = z_{m,1} + \tfrac{1}{2}\Delta s(U_1 + U_2) \tag{50}$$

$$\varphi_{m,2} = \varphi_o(s) - \frac{3}{2} U_2 \tag{51}$$

$$w'_{m,2} = 3^{\frac{1}{2}} U_2 \tag{52}$$

From (41),

$$\varphi_{i,2} = \varphi_{i,1} + \tfrac{1}{2}\Delta s \frac{w'^2_{m,2} - w'^2_{i-1,2}}{z_{m,2} - z_{i-1}} \tag{53}$$

and from (42),

$$(\log w')_{i,2} = (\log w')_{i,1} + \Delta s \left\{ \frac{\varphi_{m,2} - \varphi_{i-1,2}}{z_{m,2} - z_{i-1}} - A^2(s) \right\} \qquad (54)$$

Finally, from (49),

$$U_2 = U_1 + \tfrac{1}{2} 3^{-\frac{1}{2}} \Delta s \{ w'_{m,1} \left[\frac{\varphi_{m,1} - \varphi_{i-1,1}}{z_{m,1} - z_{i-1}} - A^2(s) \right] + U_1 \frac{w'_{m,1} - w'_{i-1,1}}{z_{m,1} - z_{i-1}} + \ldots . \} \qquad (55)$$

In (55), the additional terms correspond to those already given, but are evaluated at step 2 (figure 7b). Equations (50) to (55) are solved iteratively in the given order.

A simple finite-difference scheme to replace (45) is

$$\varphi_{-1} = -\varphi_1 , \quad \varphi_0 = 0$$
$$w'_{-1} = w'_1 \qquad (56)$$

the suffix 0 corresponding to the axis z = 0.

The initial conditions are chosen from similarity considerations. A small starting value of s is taken so that the q = 2 régime may be assumed to hold, and corresponding values of ζ_m and $\gamma = \gamma_2$ are obtained from figure 6. Then

$$z_{m,1} = \zeta^*_m s^2, \quad U_1 = 2\zeta^*_m s \qquad (57)$$

where $\zeta^*_m = \zeta_m L'/L$. Starting values of φ_m and w'_m are calculated from (51) and (52), and approximate values of $\varphi_{i,1}$ and $w'_{i,1}$ at the intermediate mesh points are found by linear interpolation from φ_m and w'_m using (56).

A plausible form for $A^2(s)$ is also based on similarity. Let

$$A^2(s) = \gamma_2/s \qquad (s < 1) \qquad (58)$$

i.e. for the duration of the q = 2 régime. Presumably the behaviour of A^2 will change at s = 1 when φ_0 (s) changes according to (44), and A^2

will begin to decrease at a slower rate. The final form must be

$$A^2(s) = \gamma_1/s \qquad (s \gg 1) \qquad (59)$$

where γ_1 ($> \gamma_2$) is chosen from figure 6 at the given ζ_m. Two simple alternative assumptions are tried here for the transition of A^2 from the form (58) to (59). Both involve taking A^2 = constant. In the first case it is assumed that the transition begins at $s = 1$, and in the second case at $s = 2$ (figure 8). Most of the actual transition probably lies within the area bounded by these two assumptions.

Although the present numerical solution does not trace characteristics, it is useful to map the backward characteristic (Γ_- in figure 8) from $z = z_m$ at $s = 1$, since this separates the $q = 2$ and transition régimes. At $z = 0$ the characteristic crosses a mirror-image characteristic (Γ_+) which has started from the opposite jump at the same instant; the second characteristic then separates the transition from the region in which the $q = 1$ régime is established. These two characteristics are traced numerically using (23).

Numerical results

Figure 8 shows two finite-difference solutions with parameter values close to the experimental values, when the wavenumber transition A^2 = constant begins (1) at $s = 1$ and (2) at $s = 2$. The similarity solutions are shown as broken lines.

In the $q = 2$ régime, the numerical solutions follow the similarity solutions quite closely, except for small wave-like perturbations which possibly arise from the starting conditions. At $s = 1$ the rate of increase in w_m' is suddenly reduced, due to the fact that φ_o has become constant. However, w_m' continues to increase because the advancing fingers contribute further to the density difference; this contribution ceases only with the arrival of the second separating characteristic, which occurs at about $s = 2$. The decrease of φ_m observed for $1 < s < 2$ is a consequence of (43). For $s > 2$ there is no further increase in density difference, and a readjustment occurs with w_m' decreasing slightly. There is little doubt that the numerical solution tends to the similarity solution for $q = 1$. The solution for z_m vs s follows similarity values very closely except in the transition region.

Figure 8 also illustrates changes of amplitude when the assumed form of the wavenumber function $A^2(s)$ is changed. The qualitative character of the solution is clearly unaffected, and the variation in z_m is probably too small to be detected experimentally.

6. CONCLUSIONS

The mechanism of mean wavenumber change is not understood. At the nose of a starting plume (section 2), an increase of scale is observed because the scale of the jet-like plume behind the nose increases as $(\kappa T)^{\frac{1}{2}}$. However, in the present problem, the fingers are so closely spaced that a scale increase is impossible without changes in the flow structure. A process of mutual entrainment might exist, the rate being controlled by diffusion, with smaller fingers generally being absorbed by the larger. There is ample experimental evidence to show that the mean wavelength increases as $(\kappa T)^{\frac{1}{2}}$.

The similarity properties seem to indicate that an equilibrium is set up as the fingers grow. Any tendency for dissipation by transverse diffusion to increase, due to increased finger length, is just balanced by the corresponding decrease in mean wavenumber.

Elder's suggestion - that acceleration continues while fluid form the diffusion layer is being drained into the fingers - provides a model which fits the observations satisfactorily. However, the process is not sufficiently well understood for either L' or L to be calculated, although the ratio $L/L' = 2$ appears to be established, and L can be measured experimentally. In the experiments described above, $L' \approx 3$ cm., and uniform fluid begins to enter the finger system when $Z_m \approx 0.65$ cm. That is, the finger amplitude at the start of the transition is quite small.

Regarding the form of equations (20) and (21), Lax (1954) was the first to show that the (weak) solutions associated with a given system depend upon the form in which the equations are written. Generally the equations and jump conditions of a hydrodynamic problem should express conservation laws and be written in the appropriate conservative forms. However, equation (21) is not a genuine conservation equation, and its correct form is not clear a priori. If, for example, (21) is written as

$$\overline{w_s^2} = 2\overline{w^2}\,(\varphi_z - \kappa_t \alpha^2/\Lambda)$$

a new set of jump conditions is obtained. The numerical solution of the new system appears to be unrelated to the experimental results.

REFERENCES

CHUOKE, R. L., VAN MEURS, P. and VAN DER POEL, C. 1959, J. Petrol. Tech. 11, 64.

DORSEY, N. E. 1940, Properties of Ordinary Water-Substance. New York: Reinhold.

ELDER, J. W. 1967, J. Fluid Mech. 27, 609.

ELDER, J. W. 1968, J. Fluid Mech. 32, 69.

FOX, L., 1962, Numerical Solution of Ordinary and Partial Differential Equations. Oxford: Pergamon.

HELLER, J. P. 1966, J. Appl. Phys. 37, 1566.

HORTON, C. W. and ROGERS, F. T. Jr., 1945, J. Appl. Phys. 16, 367.

KELLER, H. B., LEVINE, D. A. and WHITHAM, G. B. 1960, J. Fluid Mech. 7, 302.

LAMB, H. 1932, Hydrodynamics. 6th Ed. Cambridge University Press.

LAPWOOD, E. R., 1948, Proc. Camb. Phil. Soc. 44, 508.

LAX, P. D., 1954, Commun. Pure Appl. Math. 7, 159.

SAFFMAN, P. G. and Taylor, G. I., 1958, Proc. Roy. Soc. A245, 312.

SCHLICHTING, H. 1933, Zeitschr. f. angew. Math. u. Mech. 13, 260.

SLOBOD, R. L. and THOMAS, R. A. 1963, J. Soc. Petrol. Engrs. 228, 9.

TAYLOR, G. I., 1950, Proc. Roy. Soc. A 201, 192.

TAYLOR, G. I., 1953, Proc. Roy. Soc. A 219, 186.

WOODING, R. A., 1960, J. Fluid Mech. 7, 501.

WOODING, R. A. 1962, J. Fluid Mech., 13, 129.

WOODING, R. A., 1963, J. Fluid Mech. 15, 527.

CELL	I	II
Horizontal spacing of boundaries (cm)	12.0	25.45
Approximate total height (cm)	30	60
Mean plate spacing h (cm)	0.0351	0.0277
Equivalent permeability k (cm^2)	1.03×10^{-4}	6.39×10^{-5}
Width of central removable strip (cm)	0.63	1.27
Description of solute	Potassium permanganate	Potassium permanganate
Density of source solution relative to water at 18°C. $\frac{\rho_s}{\rho_w}$	1.0041	1.00695
Approximate diffusivity of source solution K (cm^2/sec)	6×10^{-6}	6×10^{-6}

Table 1. Dimensions of two Hele-Shaw cells used for experimental work, and brief descriptions of source solutions.

Table 2. Details of experimental observations plotted in figures 3 and 4. Key to plotting symbols: (a) ■, (b) ▲, (c) ◆, (d) ▼, (e) ⊕, (f) ⊛, (g) ●.

(See pages 28-34 for Tables 2a-2g, and pages 39 and 40 for Figures 3 and 4).

Elapsed time (h)	Temp. (°C)	ΔT (cm)	Mean wavelength (cm)	Mean crest-trough amplitude (cm)
0.4	15.3	1.39	1.5	0.338
0.5		1.74	1.5	0.517
0.6	15.4	2.085	1.41	0.795
0.8	15.3	2.78	1.34	1.19
1.0		3.475	1.41	1.87
1.2	15.5	4.17	1.495	2.56
1.6		5.555	1.59	4.07
2.0		6.95	1.695	5.84
2.6	15.4	9.03	1.96	8.41
3.8	15.4	13.55	2.22	12.78
4.75	15.3	16.5	2.42	16.5
6.25	15.5	21.7	2.83	20.6
8.1	15.6	28.15	2.99	26.2
9.25		32.15	3.18	27.9

Table 2(a). Cell II, $\beta = 2.^{\circ}87$, $\Lambda = 0.965 \times 10^{-3}$ cm/sec.

Elapsed time (h)	Temp. (°C)	ΔT (cm)	Mean wavelength (cm)	Mean crest-trough amplitude (cm)
0.1	14.1	0.606	0.421	0.124
0.2		1.215	0.511	0.294
0.4		2.425	0.685	0.97
0.6	14.1	3.64	0.83	2.21
0.8		4.85	0.96	2.90
1.2		7.28	1.14	4.89
1.5		9.10	1.14	6.56
1.9	14.0	11.52	1.27	7.45
2.2		13.35	1.41	8.45
2.6		15.77	1.60	10.45
3.0		18.2	1.85	10.65
3.4		20.6	1.85	11.48
3.6	14.0	21.8	1.85	13.09

Table 2(b). Cell I, $\beta = 5^{o}.42$, $\Lambda = 1.685 \times 10^{-3}$ cm/sec.

Elapsed time (h)	Temp. (°C)	ΔT (cm)	Mean wavelength (cm)	Mean crest-trough amplitude (cm)
0.2	14.3	1.354	0.463	0.271
0.3		2.03	0.613	0.532
0.4		2.71	0.727	0.782
0.5	14.3	3.38	0.807	1.33
0.6		4.06	0.82	1.79
0.8	14.3	5.41	1.00	3.23
1.0		6.76	1.11	4.56
1.25	14.5	8.45	1.24	6.39
1.5	14.6	10.15	1.30	7.95
2.0	14.6	13.54	1.50	11.00
3.0	14.8	20.3	1.96	15.5
4.0	15.0	27.0	2.32	21.8
5.0	15.0	33.8	2.55	25.8

Table 2(c). Cell II, $\beta = 5^{o}.75$, $\Lambda = 1.88 \times 10^{-3}$ cm/sec.

Elapsed time (h)	Temp. (°C)	ΔT (cm)	Mean wavelength (cm)	Mean crest-trough amplutide (cm)
0.1	15.9	1.15	0.522	0.329
0.2		2.30	0.706	1.36
0.3		3.45	0.80	2.66
0.4		4.60	0.924	4.045
0.516		5.94	1.09	5.32
0.6		6.90	1.14	6.62
0.7		8.15	1.26	7.70
0.8		9.2	1.26	8.90
1.0		11.5	1.60	11.83
1.2	16.0	13.8	1.715	13.39
1.4		16.1	1.85	13.59
1.6		18.4	1.85	14.98

Table 2(d). Cell I, $\beta = 9^{o}.82$, $\Lambda = 3.195 \times 10^{-3}$cm/sec.

Elapsed time (h)	Temp. (°C)	ΔT (cm)	Mean wavelength (cm)	Mean crest-trough amplitude (cm)
0.15		2.08	0.471	
0.2	15.6	2.78	0.572	0.762
0.25		3.47	0.667	1.597
0.3		4.16	0.685	2.14
0.4	15.6	5.55	0.705	3.70
0.5		6.94	0.80	5.30
0.583		8.10	0.857	6.50
0.8	15.5	11.10	1.04	9.48
1.0	15.6	13.89	1.14	12.50
1.5	15.6	20.82	1.33	16.9

Table 2(e). Cell II, $\beta = 11^{\circ}.5$, $\Lambda = 3.855 \times 10^{-3}$ cm/sec.

Elapsed time (h)	Temp. (°C)	ΔT (cm)	Mean wavelength (cm)	Mean crest-trough amplutide (cm)
0.0583	14.6	1.62	0.335	0.59
0.1		2.78	0.428	1.22
0.125		3.475	0.509	2.07
0.142		3.95	0.525	2.48
0.158		4.39	0.547	3.16
0.175		4.87	0.585	3.56
0.2		5.56	0.599	4.35
0.258	14.6	7.18	0.687	6.28
0.3		8.35	0.750	7.22
0.4		11.13	0.807	10.24
0.5		13.90	0.848	13.41
0.6		16.69		15.42
0.8	14.6	22.25		21.3
1.0		27.8		24.7
1.25	14.6	34.75		31.7

Table 2(f). Cell II, $\beta = 24^{\circ}.5$, $\Lambda = 7.725$ cm/sec.

Elapsed time (h)	Temp. (°C)	ΔT (cm)	Mean wavelength (cm)	Mean crest-trough amplitude (cm)
0.0167		0.95	0.284	0.120
0.0333		1.89	0.288	0.439
0.05		2.85	0.322	1.316
0.0667		3.79	0.388	2.25
0.0833		4.73	0.458	3.29
0.1		5.69	0.480	4.41
0.1333		7.60	0.509	6.58
0.15		8.54	0.530	7.44
0.2	16.5	11.38	0.572	10.70
0.25		14.21		14.45
0.3		17.07		15.78
0.4		22.7		22.8
0.5		28.4		27.48

Table 2(g). Cell II, $\beta = 55^{\circ}.9$, $\Lambda = 15.8 \times 10^{-3}$ cm/sec.

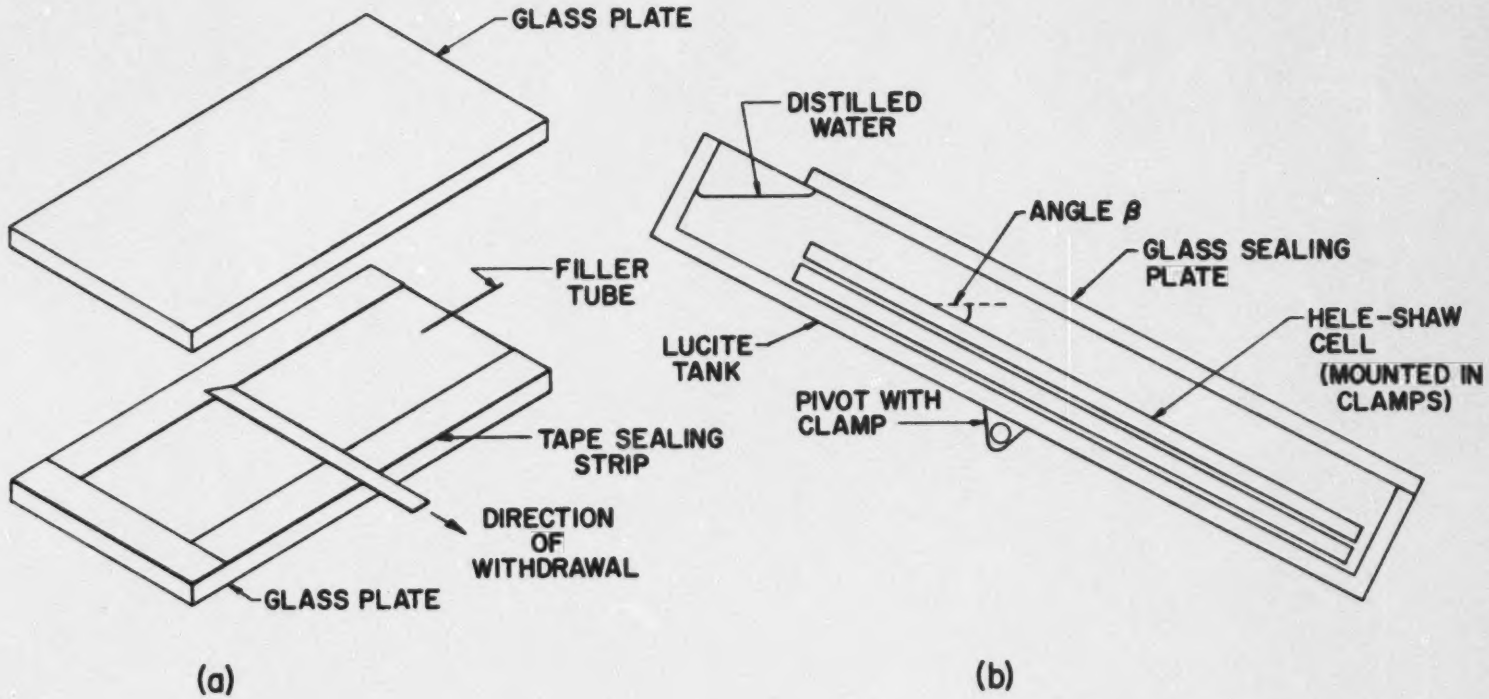

(a) Construction of cell. (b) Tilted tank containing cell.

Fig. 1. Hele-Shaw cell apparatus for producing fingers at an unstable diffusing interface.

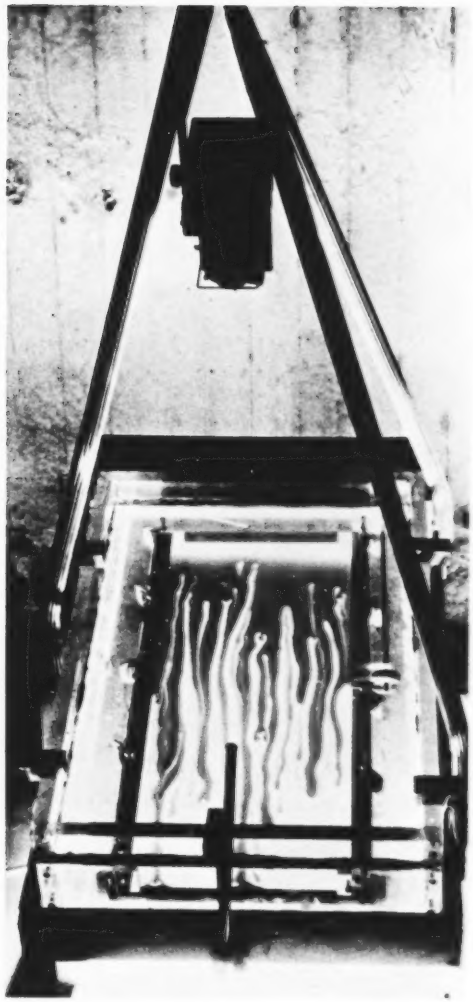

Fig. 1(c). General view of Hele-Shaw apparatus.

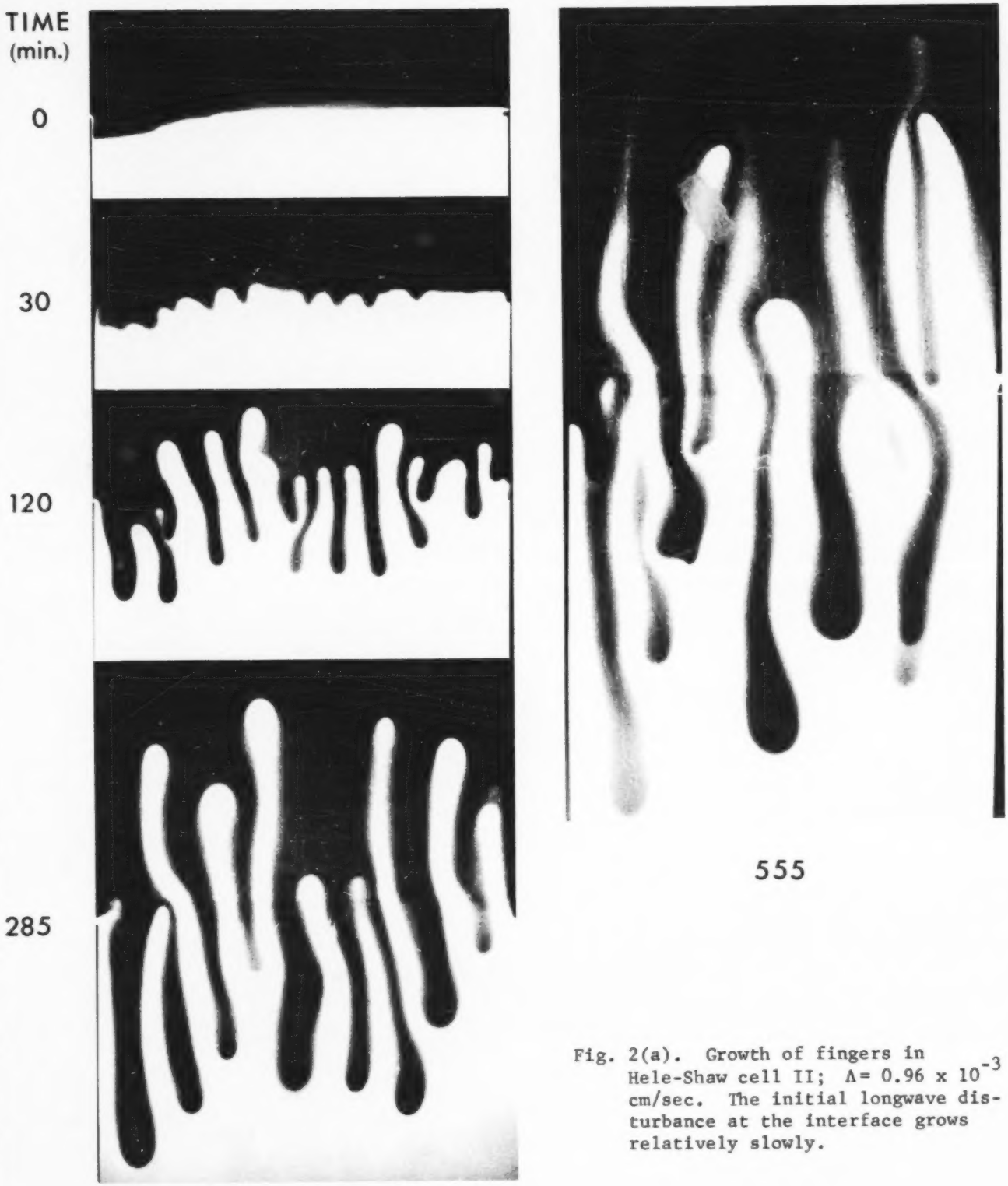

Fig. 2(a). Growth of fingers in Hele-Shaw cell II; $\Lambda = 0.96 \times 10^{-3}$ cm/sec. The initial longwave disturbance at the interface grows relatively slowly.

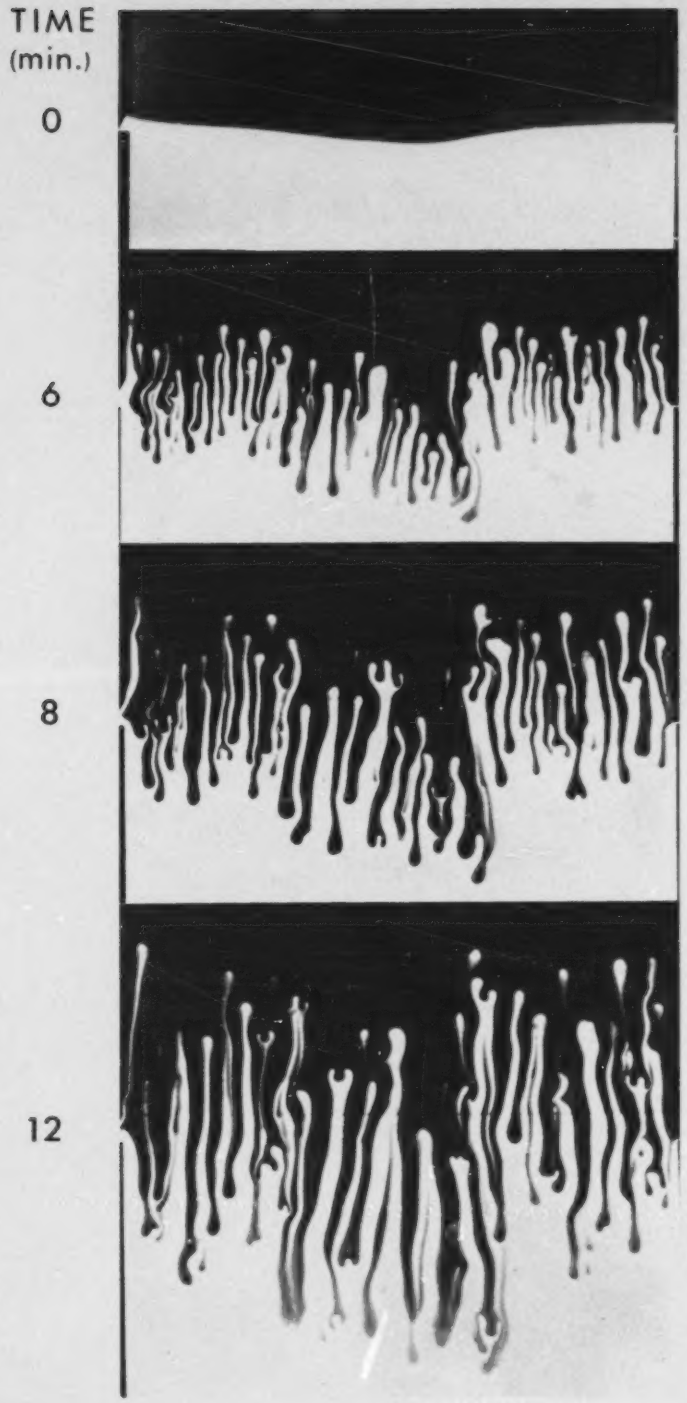

Fig. 2(b). Break-up of finger fronts due to instability. Cell II; $\Lambda = 15.8 \times 10^{-3}$ cm/sec. This process was observed within the experimental range for $\Lambda > 5 \times 10^{-3}$ cm/sec.

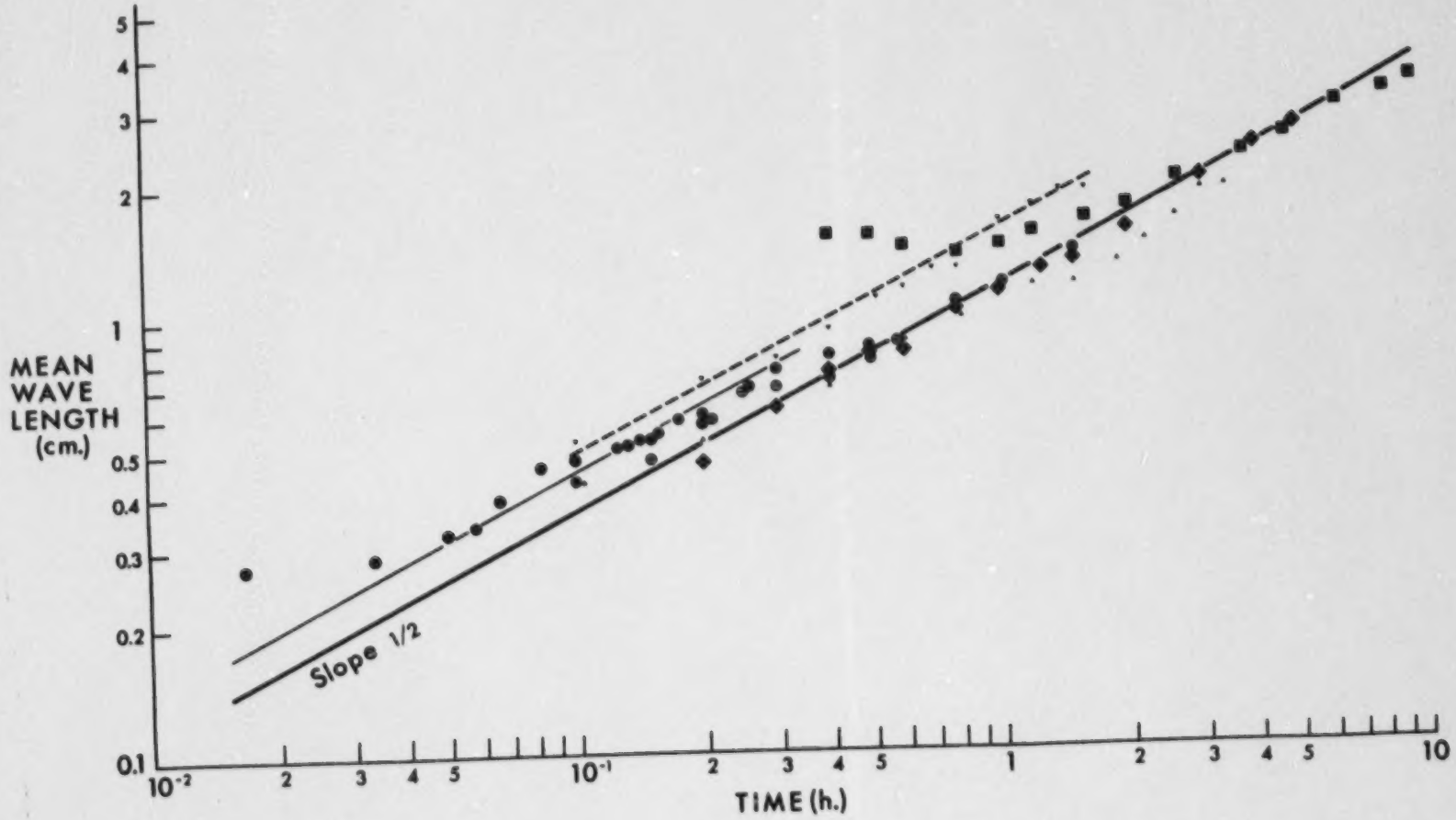

Fig. 3. Mean wavelength vs. time measured from 7 experiments with parameters given in Table 2. Heavy full line: mean wavelength measured in q = 1 regime (section 4). Thin full line: mean wavelength calculated for q = 2 regime. Broken line: mean wavelength measured in anomalous experiment using cell I. (See page 27 for definition of symbols.)

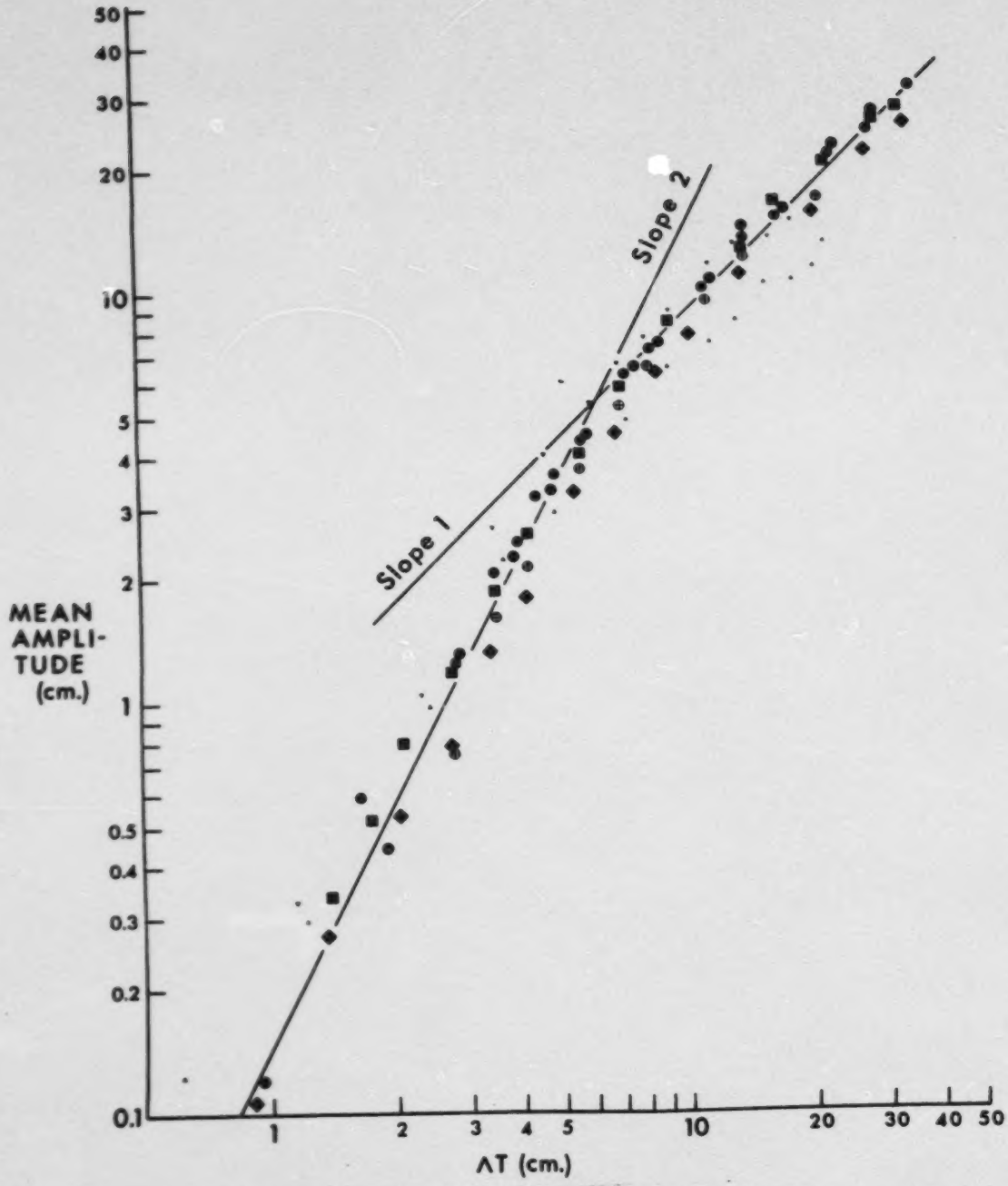

Fig. 4. Mean crest-trough amplitude vs. $\Delta T = S$ measured from 7 experiments with parameters given in Table 2. Straight full lines have been drawn to represent the $q = 1$ and $q = 2$ regimes (section 4). (See page 27 for definition of symbols.)

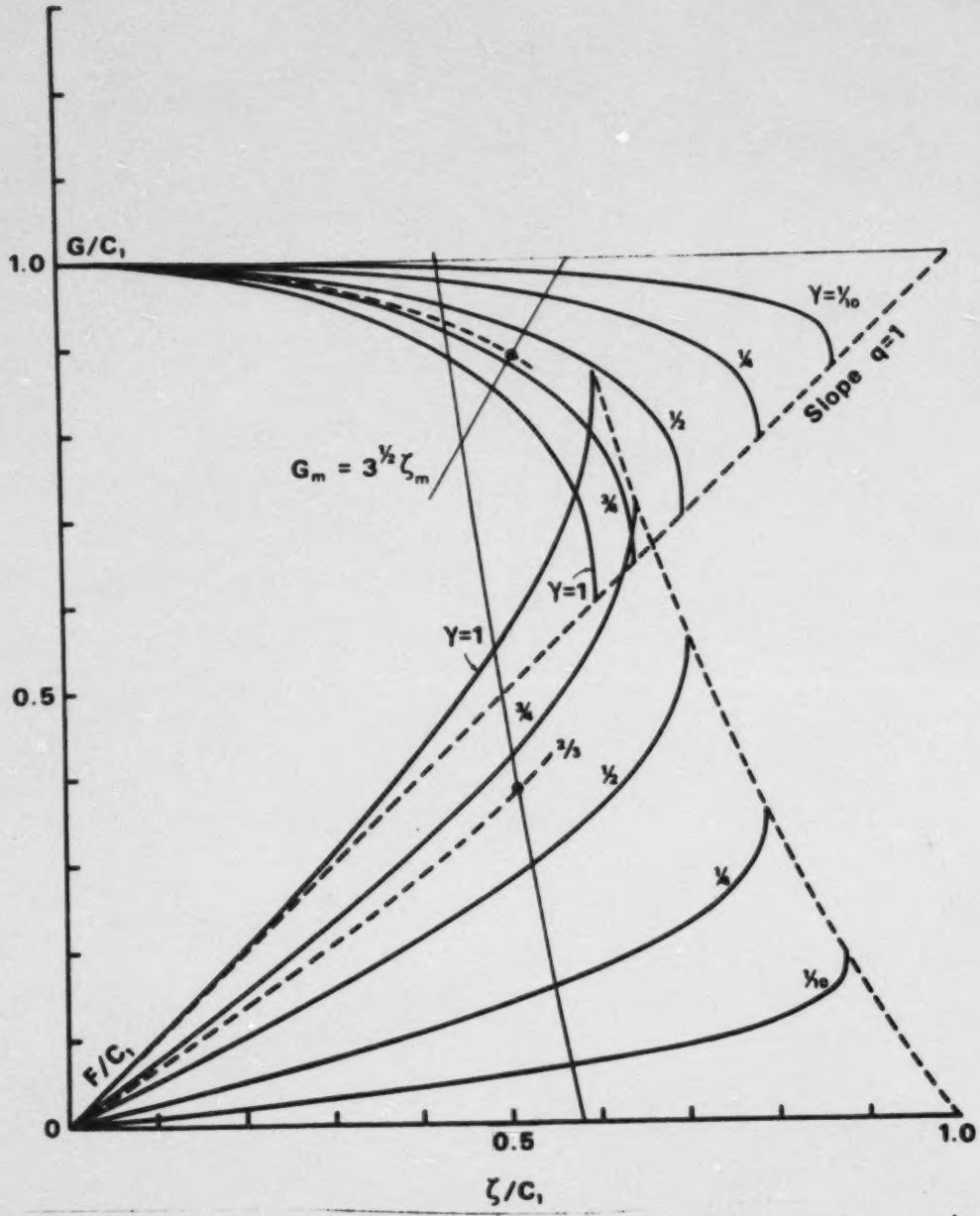

Fig. 5(a). Solution curves for the similarity variables F/C and G/C as function of ζ/C. A jump condition (32) relating ζ_m and G_m is represented by a thin line which, if produced, would pass through the origin. A second thin line indicates the corresponding values of F_m. The jump condition in (32) involving $F_\rho - F_m$ sets C. Broken curves and black circles correspond to experimental values: $q = 1$, $C = C_1$.

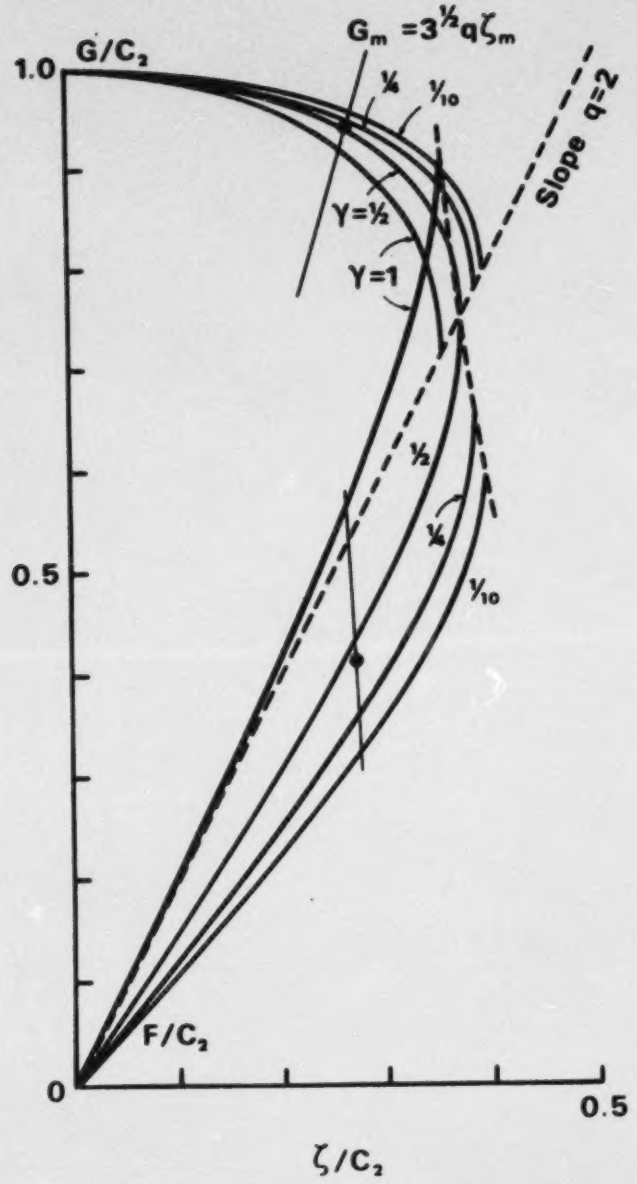

Fig. 5(b). Solution curves for the similarity variables F/C and G/C as function of ζ/C. A jump condition (32) relating ζ_m and G_m is represented by a thin full line which, if produced, would pass through the origin. A second thin line indicates the corresponding values of F_m. The jump condition in (32) involving $F_o - F_m$ sets C. Broken curves and black circles correspond to experimental values: $q = 2$, $C = C_2$.

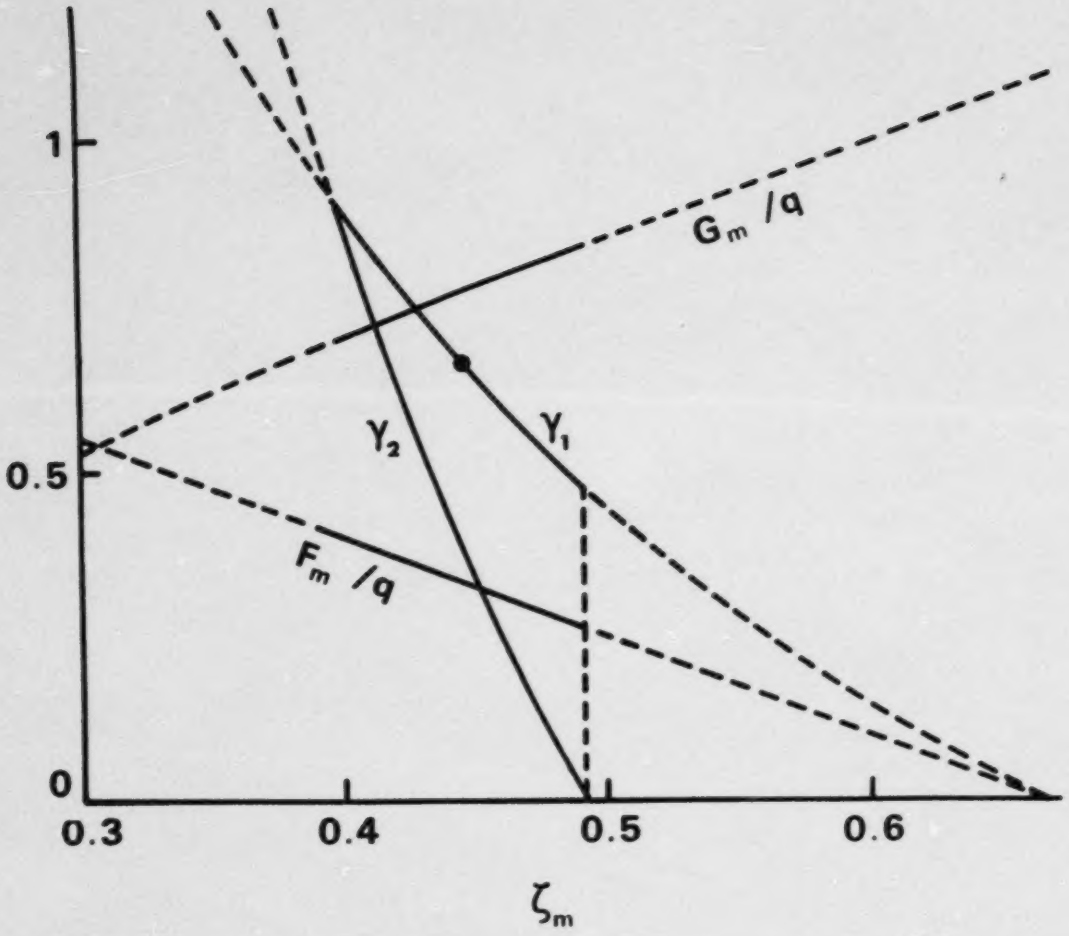

Fig. 6. F_m/q, G_m/q and γ_q, where $q = 1,2$, as functions of ζ_m. By definition ζ_m has the same value for both regimes, so that γ must undergo a transition $\gamma_2 \rightarrow \gamma_1$.

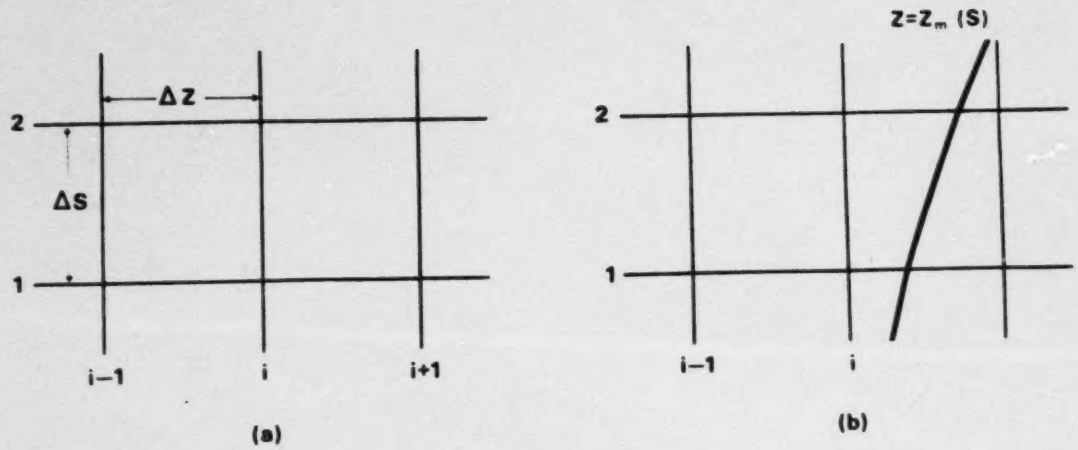

Fig. 7. (a) Finite-difference mesh used in the (s,z)-plane.
(b) Representation of the jump in the finite-difference scheme.

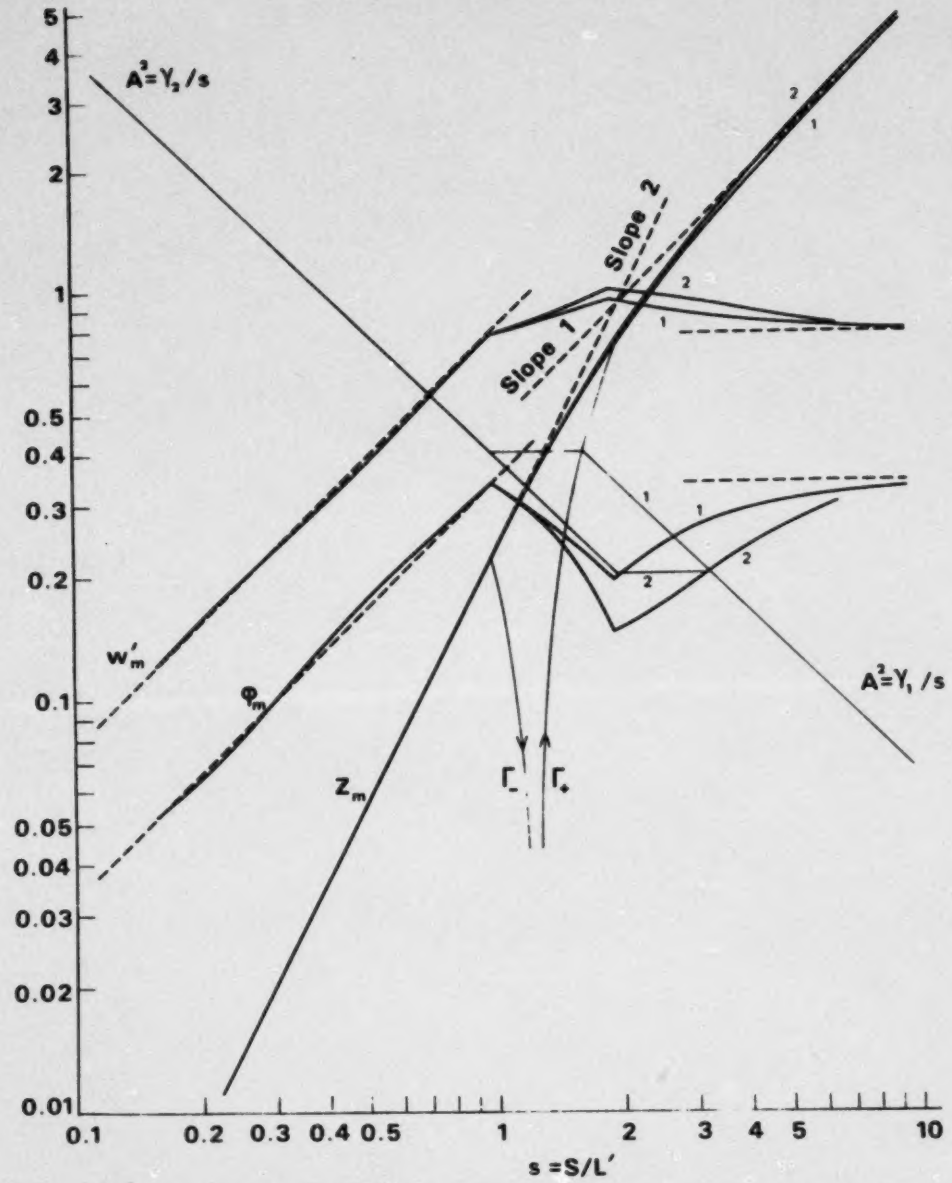

Fig. 8. Numerical solution (full lines) of equations (41) and (42), subject to conditions (43) to (45), using the methods of Lax (1954) and Keller, Levine and Whitham (1960). Similarity solutions are shown as broken lines. The numerals 1,2 identify two alternative assumptions for the transition of γ. Γ_+ denote ascending and descending characteristics which originate at the beginning of the transition. Parameter values: $\zeta_m = 0.444$ (cf. (18) and figure 6), $\gamma_1 = 0.667$, $\gamma_2 = 0.40$, $L' = \frac{1}{2} L = 3.05$ cm.